APPLICATION OF GEOPHYSICAL METHODS AND EARTHQUAKE ENGINEERING TO SEISMOGENIC LANDSLIDES AND FAULT SCARPS IN KYRGYZSTAN (CENTRAL ASIA)

H.-B. Havenith[1] , D. Jongmans[1], K. Abdrakhmatov[2], I. Torgoev[3], D. Delvaux[4], P. Trefois[4], A. Strom[5], V. Losev[3], S. Geeninckx[1], Y.G. Alioshin[3], I. Lemzin[2], C. Tulegen[2]

[1]: Laboratory of Geophysics, University of Liege, Liege
[2]: Kyrgyz Institute of Seismology, Bishkek
[3]: Institute of Physics and Mechanics of Rocks, National Academy of Sciences, Bishkek
[4]: Department of Geology, Royal Museum of Central Africa, 3080 Tervuren
[5]: Hydroproject Institute, Moscow.
Belgium, Kyrgyz Republic, Russia

Summary

Different kinds of geophysical methods were applied to three case studies in the northern Tien Shan : two rock avalanches near Bielogorka (50 km Southwest of Bishkek), a complex debris slump in the Suusamyr valley (130 km Southwest of Bishkek) and a rock avalanche near Ananevo. The two latter sites are very close to the fault. On the Ananevo rock avalanche, an intensive field study combined refraction seismics and a seismological experiment in order to define amplification effects of the ground motions in the site. We compare also the experimental study with 2D Finite-Element modelling of the ground motion in the Ananevo landslide site.

The sites

In the frame of the project 'Landslides triggered by earthquakes in Kyrgyzstan, Tien Shan' two field trips had been organised in the northern Tien Shan in order to study three landslides sites : two rock avalanches near Bielogorka, a debris slump in the Suusamyr valley and a rock avalanche north of Ananevo. The location of the sites is shown in figure 1.

НАЦИОНАЛЬНАЯ АКАДЕМИЯ НАУК
КЫРГЫЗСКОЙ РЕСПУБЛИКИ

ИНСТИТУТ ФИЗИКИ И
МЕХАНИКИ ГОРНЫХ ПОРОД

ПРОБЛЕМЫ ГЕОМЕХАНИКИ И ГЕОТЕХНИЧЕСКОГО ОСВОЕНИЯ ГОРНЫХ ТЕРРИТОРИЙ

Труды международной конференции,
посвященной 40-летию ИФиМГП НАН КР
и международному Году гор
(Бишкек, 4–6 октября 2000 г.)

Под общей редакцией
академика НАН КР,
профессора *И.Т. Айтматова*

Издательство «Илим»
Бишкек • 2001

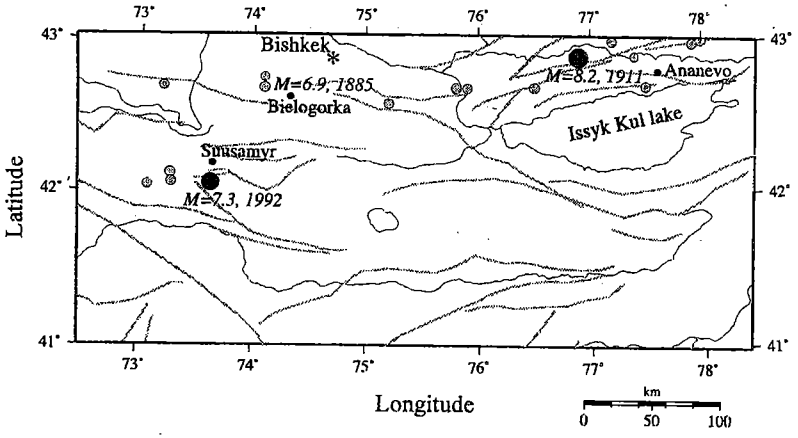

Figure 1: Location of the three landslide sites and of the assumed triggering earthquakes in the northern Tien Shan.

The Bielogorka rock avalanches

The Bielogorka rock avalanches (Figure 2) are supposed to have been triggered by the 1889 Bielovodskoe earthquake (assumed Magnitude of 6.9), but the seismic origin is not yet proved beyond doubt.

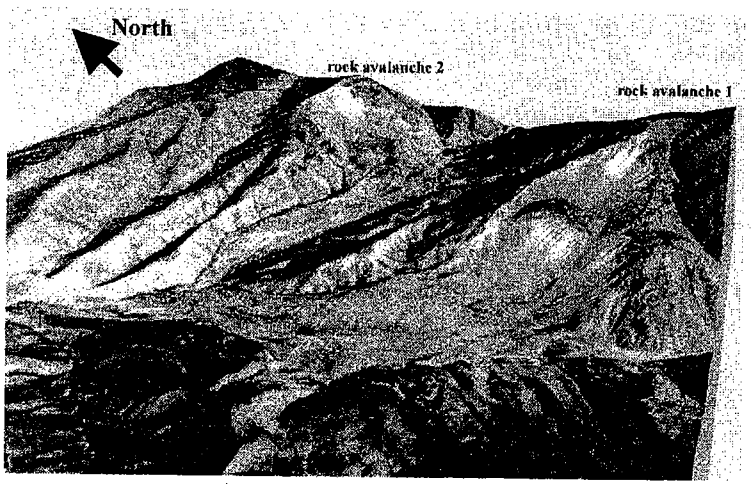

Figure 2: Digital elevation model of the two rock avalanches at Bielogorka.

They are the biggest landslides we visited and have a volume of 5 to 10 Mio. of m³. Only rock avalanche 1 (Figure 2) has been investigated by geophysics, principally seismic sounding in order to determine the depth and geometry of the displaced material. By there the geophysical results allowed to reconstruct the topography previous to the failure.

Simple pseudo-static slope stability calculations using Janbu's method (Janbu, 1973) were applied to the pre-failure slope and allowed to define a factor of safety (FS) of about 2. An additional horizontal seismic acceleration of 0.3 g is needed to cause instability, which indicates the high probability of a seismic triggering of the Bielogorka avalanches.

The Suusamyr site

During the 1992 Suusamyr earthquake of a Ms=7.3, landslides as well as other ground failures were triggered on the south-facing slope and on the crest of the Chet-Korumdy ridge (Figure 3a). The landslides can be classified as debris slumps, debris flows or may present a combination of these two types of movements. In addition, fresh scarps were observed on old landslides, which indicates their recent reactivation in 1992.

Our case study was focused on the largest, newly formed landslide (Figure 3b), of a volume of 0.5 to 1 106 m³. In its upper part, below the 50 m high main scarp, the landslide consists of a multi-rotational debris slump. Several secondary scarps formed on the body of the slump due to the lateral spreading of the debris material that turned into a debris flow in the lowest part of the landslide.

Besides the other smaller landslides presenting a less complex structure, different fracture patterns affect the southern slope of the ridge (Figure 3b). Several of them have been observed on air-photographs prior to the 1992 earthquake and are therefore not related to this event. At the crest of the ridge, a gravitational graben, 10 m wide and extending over more than 100 m along the crest, formed during the earthquake between a main south-facing and secondary north-facing scarps. North of the crest, no significant surface effects have been detected.

At the bottom of the Suusamyr valley, surface faulting related to the 1992 earthquake formed several scarps in alluvial deposits, the main fault scarp being up to 2.5 m high and 500 m long (Figure 7) . The distance between the above-mentioned landslides and the fault scarp is less than 5km.

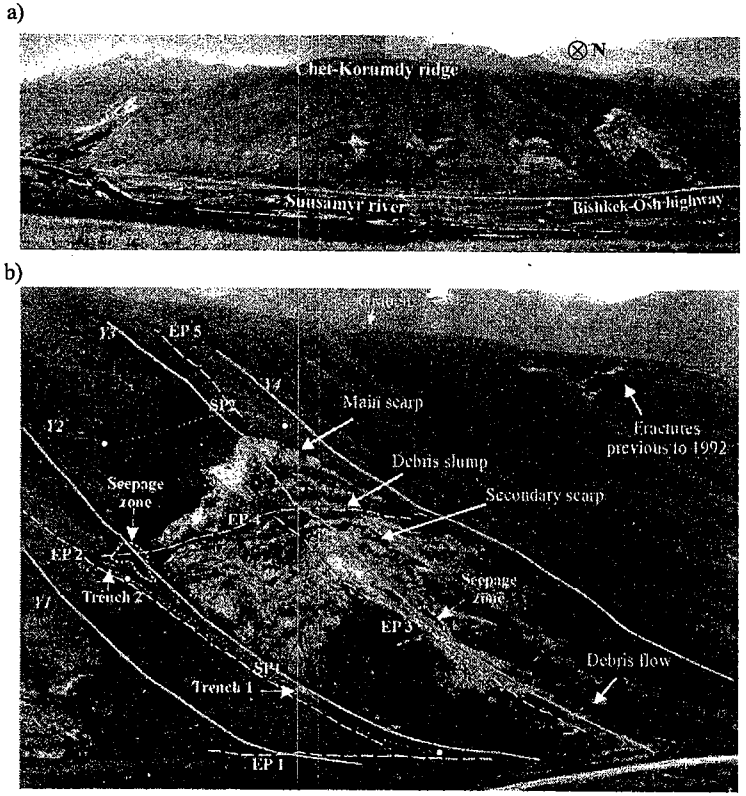

Figure 3: a) Surface effects on the south-facing slope of the Chet-Korumdy ridge triggered by the Ms=7.3 Suusamyr earthquake in 1992. c) Detailed view on the investigated landslide showing electrical profiles (EP) and seismic profiles (SP), Y1-Y4 sections (see also Figure 5) and two trenches are indicated.

The Suusamyr debris slump has been studied by electrical tomography and seismic sounding. The geophysical data were readily calibrated by observations of slope materials in two 2.5m deep trenches (Figure 4) : black soil, reddish arenites and brown silty clays were observed in these trenches. On the tomography EP2 shown in Figure 4b the location of the contact between the arenites and the silty clays corresponds to the 70 Ωm contour line; arenites have a resistivity higher than 70 Ωm while silty clays are less resistive. This contour was used on the geoelectric section across the debris slump (Figure 4a) to outline the landslide mass, which was observed as mainly made of arenites. A third lithology underlying the arenites and silty was

defined on two seismic profiles performed close to the landslide. One of the profiles runs along the tomography EP2 and is shown in Figure 3b. The deepest layer of P-velocity of more than 3000 m/s in fact corresponds to Neogene sediments observed on outcrops in the Suusamyr valley.

Combining all geophysical and geotechnical data, a three dimensional geological model of the landslide was built. The main longitudinal section Y3 (Figure 5a) of the model was then used for pseudo-static slope stability computations, which show that under static conditions the slope is nearly unstable with a FS of 1.14.

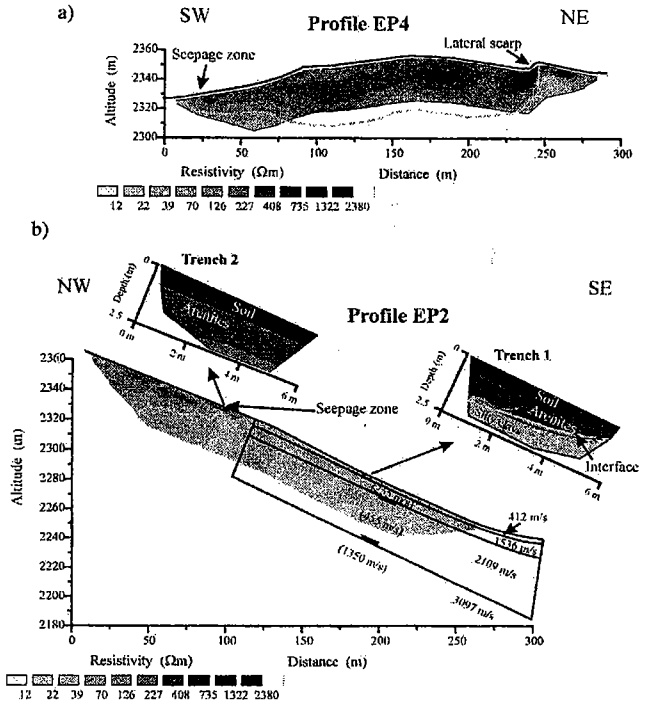

Figure 4: a) Geoelectric profile EP4 across the upper portion of the debris slump. The light contour line (70 Ωm) indicates the approximate contact between arenites and silty clays, the dashed line corresponds to its extrapolation below the investigation depth. b) Electrical tomography EP2 and seismic profile SP1 located at 100 m to the West of the landslide. Schematic view of the two trenches show the observed lithologies, the ground water level (trench 2) as well as the projection of the 70 Ωm contour line. Along the seismic profile SP1 are indicated P-velocities and S-velocities (in brackets) of the layers.

A horizontal acceleration of 0.05g induces instability. An accelerogram was simulated for the site using the source characteristics of the 1992 Suusamyr earthquake (Figure 5c). The Newmark displacement (Newmark, 1965) calculated for this accelerogram and for a critical acceleration of 0.05 g amounts to only 0.06 m (Figure 5d). This value is very small compared with the actual 70 m o displacement of the debris slump baricenter. The main reason for this is that the Newmark displacement does neither take into account real dynamical effects nor the post-seismic displacements. Yet, by introducing site amplification effects estimated by modelling the 1D-site response (Figure 5b and 5e), it was possible to increase the Newmark displacement by a factor of 10 (Figure 5f). However, the final 0.6 m of displacement are still much less than the real one.

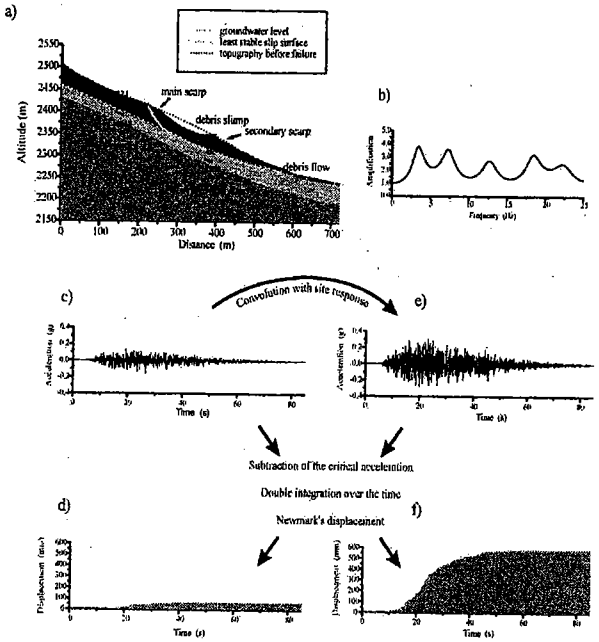

Figure 6: a) Geological section (corresponding to section Y3 on Figure 2c) used for static and pseudo-static slope stability calculations using Janbu's method. The graph also displays the Vs models of two seismic profiles projected on the section. b) 1D theoretical amplification for the Vs model 1 in Figure 8a. c) Accelerogram simulated at 5 km from the fault rupture related to the Ms=7.3 Suusamyr earthquake. d) Newmark displacement calculated for the accelerogram (b) and for a critical acceleration of 0.05g. e) Accelerogram in (c) convoluted with the 1D theoretical site response calculated for the Vs model 1. f) Newmark displacement for the convoluted accelerogram.

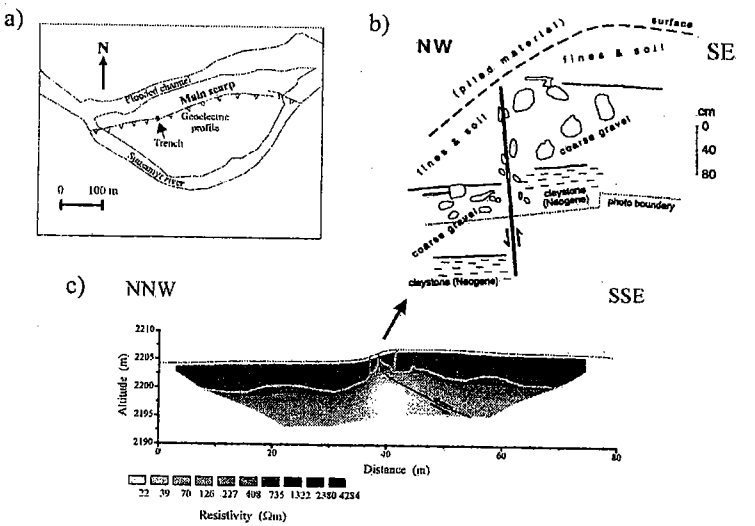

Figure 7: a) Sketch showing the localisation of the geoelectric profile across the fault scarp and the trench made by Korjenkov et al. (1999). b) Drawing of the fault observed in the trench (Korjenkov et al. 1999). c) Resistivity section across the main fault scarp with indication of the inferred lithological contact (white line) between alluvial deposits (above) and Neogene sediments (below) and the fault mechanism.

In addition to the geophysical investigation of the landslide, an electrical profile was also executed across the main fault scarp at the bottom of the valley in order to investigate the fault geometry at depth. The location of the profile and the resistivity section are shown in Figure 7a and 7b. The electrical data (Figure 7b) could be calibrated by observations in trench across the fault scarp (Figure 7c) made by Korjenkov et al. (1999). The superficial high resistivities are related to alluvial deposits, mainly large boulders poorly cemented by silts or clays overlying the Neogene sediments composed of claystone. The observations in the trench indicate that the contact between the layers can be located around the1300 Ωm (light) contour. Figure 7c reveals that there is a clear difference of altitude (about 1.5 m) along the contour close to the fault scarp in relation to the thrusting of the southern block over the northern (Figure 7b, Korjenkov et al. 1999).

The Ananevo rock avalanche

The last case study concerns the Ananevo rock avalanche triggered in 1911 by the M=8.2 Kemin earthquake. The avalanche lies just above the seismogenic thrust fault activated in 1911 crossing it at his foot from NW to SE (Figure 8).

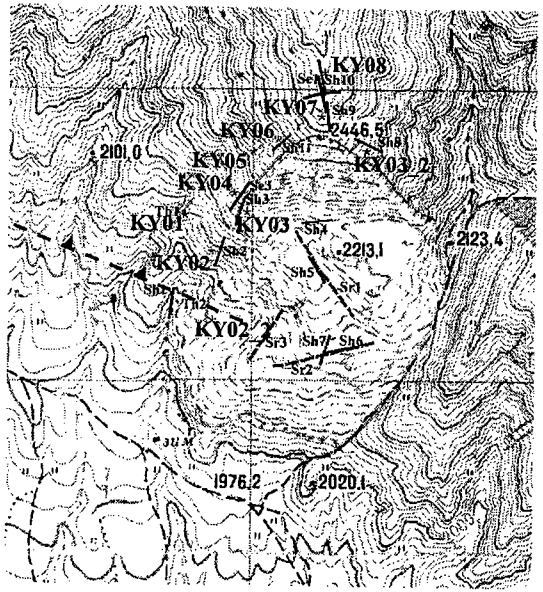

Figure 8: Map of the Ananevo rock avalanche with location of the seismic soundings and of the seismological stations.

The investigations included seismic soundings and seismic tomographies (see Figure 8 for location), geotechnical in situ and laboratory tests, as well as an extended seismological survey. Seismic tomographic profiles were also performed on two sites along the southern branch of the Kemin fault (north of the Issyk Kul lake) and on the scarp of the main fault activated in 1911, near to the fatal Tchon Kemin rock avalanche triggered by the same earthquake.

The rock avalanche developed in Palaeozoic granite deeply weathered as evinced by the low P-velocities of less than 2000m/s measured in the vicinity of the avalanche. Particularly at the crest the depth of weathering exceeds 70 m (the maximum investigation depth) as shown a seismic sounding along the crest presented in Figures 9. P-velocities and associated S-velocities determined by surface wave inversion (Figure 9) are respectively about 900m/s and 600m/s at a depth of 30m. At the same depth along the slope, the P-and S-velocities are somewhat higher, respectively 1200m/s and 800m/s.

In situ ultra-sound measurements on granite monoliths showed compressional wave velocities of about 1000 to 2000m/s. Comparing these values with P-velocities near the surface (of less than 500m/s), it appears that

the low P-velocities measured by seismic sounding are due to strong fracturing of the rock. In addition a structural study of fracture systems around the site indicates that fracturing clearly influenced the failure both by inducing a low shear and compressional strength of the rock and by an unfavourable orientation with regard to the topography. On the base of mean Vp and Vs values per layer, a global Poisson ratio of about 0.29 and an Ed module per layer were calculated. The Ed modules of the seismic layers range between 825 MPa near the surface and 26000 MPa at a depth below 50m.

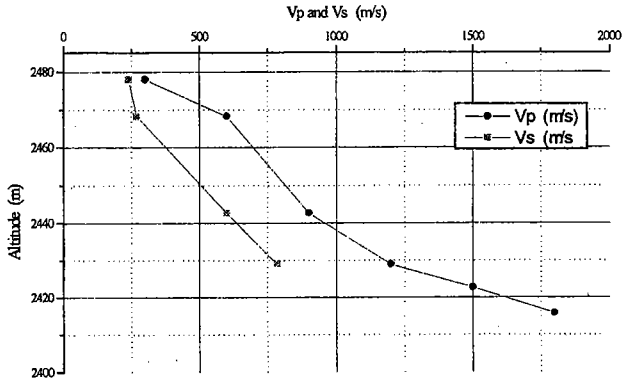

Figure 9: a) Seismic sounding showing P- and S-velocities along the crest above the rock avalanche.

From a dynamical point of view, both experimental data of 100 recordings of earthquakes at 8 seismological stations and finite element modelling of the ground motion indicated a strong spatial variation of the ground motion along the slope. Amplification is increased at the foot of the slope and on the crest (Figure 10).

Both topographical and surface layer effects can be observed. The strong amplification of the ground motion close to the crest (Figure 10e and 10f) may be a major factor of the failure at the origin of the avalanche as it was shown in the previous paragraph (Figure 7) that the amplification significantly increases the Newmark displacement.

A great range of compressional and shear strength values were measured or taken from references (Hoek and Bray, 1981) for the different types of granites cropping out in the vicinity of the rock avalanche. Therefore the static FS is not very constrained, but in all cases indicates static stability with a critical acceleration greater than 0.1g.

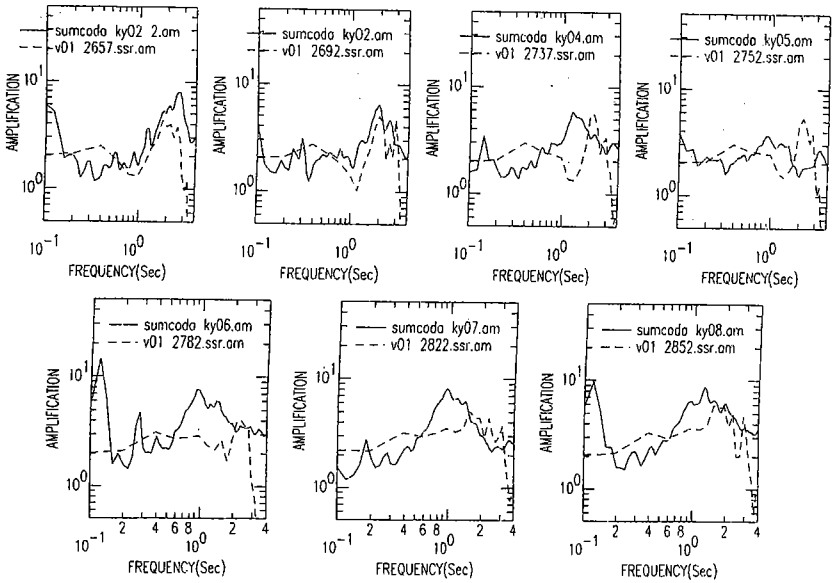

Figure 10: H/V ratios (solid lines) at seven seismological stations (ky02_2, ky02, ky04, ky05, ky06, ky07, ky08 : see Figure 8 for location) indicating the amplification over a frequency range up to 4 Hz. Comparison with FE modelling results (dashed lines).

The fault zone at the foot of the avalanche could be observed over 10 to 20 m. It is characterised by highly fractured and weathered rock. 5 km NW of the avalanche and in the Tchon Aksu valley surface ruptures associated to this fault was studied by seismic tomography. In the Tchon Kemin valley three seismic tomography profiles were realised across the Tchon-Kemin fault scarp. One of these profiles is shown in Figure 11.

References

1. *Hoek, E. and Bray, J.* (1981). Rock slope engineering. Institution of Mining and metallurgy, pp.358.
2. *Janbu, N.* (1973). Slope stability computations – Embankment – Dam Engineering. Casagrande Volume, Wiley, New York.
3. *Korjenkov, A., Bowman, D., Haselton, K.* and *Porat, N.* (1999). Recent drainage diversions under thrusting conditions in the Suusamyr valley, the Tien Shan Range, Kyrgyzstan. Isr.Jour.Earth Sci., vol. 48, 63–79.
4. *Newmark, N.* : (1965). Effects of earthquakes on dams and embankments. Géotechnique, 15, 2, 137–160.

PROBABILISTIC SEISMIC HAZARD MAP OF KYRGYZSTAN (CENTRAL ASIA): APPLICATION TO THE REGIONAL HAZARD OF SEISMICALLY INDUCED LANDSLIDES

H.-B. Havenith[1], Philippe Trefois[2], D. Jongmans[1], K. Abdrakhmatov[3], D. Delvaux[2]

[1]: Laboratory of Geophysics, University of Liege, Liege
[2]: Department of Geology, Royal Museum of Central Africa, Tervuren
[3]: Kyrgyz Institute of Seismology, Bishkek

Belgium, Kyrgyz Republic

Summary

In the frame of the project called 'Landslides triggered by earthquakes in Kyrgyzstan, Tien Shan' different probabilistic seismic hazard maps of Kyrgyzstan were built. While PGA maps are important for civil engineering structures, Arias intensity maps are used as input for hazard calculations of seismogenic landslides. On a GIS platform, the Arias intensity map as well as geotechnical, geological and morphological information were compiled to estimate the hazard of seismically induced landslides for the Suusamyr region, Kyrgyzstan. We applied the method of Jibson et al. (1998) using the concept of the Newmark displacement.

Seismic zones and their activity

The seismic catalogue of Kyrgyzstan contains data of more than 69000 earthquakes. The whole catalogue covers a period of about 2250 years, with historical data beginning in 250 BP and first instrumental records beginning in 1960. The data of this catalogue as well as geological and tectonic information were compiled to outline two types of seismic zones.

At first, Kyrgyzstan was divided in six large tectonic zones : northern Tien Shan, northeastern Tien Shan, central Tien Shan, southeastern Tien Shan - northern Tarim basin, southern Tien Shan - northern Pamir and finally the western Tien Shan (Figure 1).

Secondly, inside these large areas, zones of an increased historical and instrumental seismicity have been outlined (Figure 1). The extension of these smaller zones is directly depending on fault traces that have been studied on satellite images as well as on geological maps. In the northern Tien Shan area, mainly three zones present a higher seismicity : the southern Chu basin